Remote Sensing of Precipitation Using Reflected GNSS Signals: Response Analysis of Polarimetric Observations

Milad Asgarimehr, Mostafa Hoseini, Maximilian Semmling, Markus Ramatschi, Adriano Camps, *Fellow, IEEE*, Hossein Nahavandchi, Rüdiger Haas, and Jens Wickert

***Abstract*— For the first time, rain effects on the polarimetric observations of the global navigation satellite system reflectometry (GNSS-R) are investigated. The physical feasibility of tracking the modifications in the surface roughness by rain splash and the surface salinity by the accumulation of freshwater is theoretically discussed. An empirical analysis is carried out using measurements of a coastal GNSS-R station with two side-looking antennas in right- and left-handed circular polarizations (RHCP and LHCP). Discernible drops in RHCP and LHCP powers are observed during rain over a calm sea. The power drop becomes larger at higher elevation angles. The average LHCP power drops by ≈ 5 dB at an elevation angle of 45°. The amplitude of the correlation sum shows a dampening, responding to rain rate systematically. The LHCP observations show higher sensitivity to rainfall compared to RHCP observations. The retrieved standard deviation of surface heights shows a steady increase in the rain rate. The derived surface salinity shows a decrease for rains higher than 10 mm/h. This study confirms the potential under environmental conditions of the GNSS-R ground-based station, e.g., with salinity mostly lower than 30 psu, over a calm sea, being a starting point for future investigations.**

***Index Terms*— GNSS-reflectometry (GNSS-R), polarimetric observations, rain, sea surface salinity (SSS), surface-roughening.**

I. Introduction

THE dependence of human beings on precipitation as a freshwater resource is clear. This component of the water cycle plays a key role in the economy and sustainable developments. Scarce or extreme rainfalls can lead to droughts or floods, threatening lives and properties. Besides, global warming is expected to change the extreme precipitation patterns in terms of magnitude and frequency [1]. Monitoring global precipitation events can assist scientists to better recognize the climate change patterns.

In situ measurements and weather radars are the traditional methods to measure precipitation. They provide the required precipitation information for regional-scale studies, where a dense network of these instruments is established. These techniques are not able to capture the global precipitation due to the coverage limitations, especially over oceans and regions with underdeveloped infrastructures. To this end, meteorological satellites are used that are mainly equipped with advanced microwave and infrared instruments. The tropical rainfall measuring mission (TRMM) was one of the key satellites that contributed to improving our knowledge on the distribution and variability of precipitation within the tropics, operating from 1997 to 2015 [2]. The global precipitation measurement (GPM) mission refers to a network of next-generation satellites providing precipitation information [3]. The GPM core observatory was launched in 2014 carrying a microwave radiometer. The GPM centers bring precipitation observations from the operational satellites together and provide the standard data products. In [4], a review of the precipitation data sources and instruments is provided.

The exploitation of reflected global navigation satellite system (GNSS) signals from the Earth's surface, so-called GNSS-reflectometry (GNSS-R), has emerged as a powerful technique to obtain a variety of geophysical parameters and surface properties, see, e.g., [5]. The GNSS-R technique is a multistatic radar method using existing signals from numerous GNSS satellites as the transmitters. The small and cost-effective receivers can be implemented at ground-based stations or onboard different air/spaceborne platforms such as satellites. The cyclone GNSS (CYGNSS) is a constellation of eight low Earth orbiting (LEO) microsatellites, launched in December 2016, fully dedicated to GNSS-R [6]. Given the proven capabilities of GNSS-R to obtain a variety of surface and atmospheric parameters, precipitation monitoring can be a novel application of GNSS-R, which still needs investigations to enhance the knowledge on interactions between rain and the air-sea interface and consequently their impact on GNSS-R measurements. Due to the novelty of the technique, a very limited number of studies discuss the rain effects on GNSS-R observations, and this process is not yet well understood.

AQ:1 Manuscript received December 7, 2020; revised January 20, 2021; accepted February 15, 2021. This work was supported by the German Research Centre for Geosciences (GFZ), Potsdam, Germany. *(Corresponding author: Milad Asgarimehr.)*

AQ:2 Milad Asgarimehr and Markus Ramatschi are with the German Research Centre for Geosciences (GFZ), 14473 Potsdam, Germany (e-mail: milad.asgarimehr@gfz-potsdam.de).

Mostafa Hoseini and Hossein Nahavandchi are with the Department of Civil and Environmental Engineering, Norwegian University of Science and Technology, 7491 Trondheim, Norway.

Maximilian Semmling is with the Institute for Solar-Terrestrial Physics, German Aerospace Center (DLR), 17235 Neustrelitz, Germany.

Adriano Camps is with the CommSensLab-UPC, Department of Signal Theory and Communications, UPC BarcelonaTech, 08034 Barcelona, Spain, and also with the Institut d'Estudis Espacials de Catalunya (IEEC/CTE), Universitat Politècnica de Catalunya (UPC), 08034 Barcelona, Spain.

Rüdiger Haas is with the Department of Space, Earth and Environment, Chalmers University of Technology, 41296 Gothenburg, Sweden.

Jens Wickert is with the German Research Centre for Geosciences (GFZ), 14473 Potsdam, Germany, and also with the Institute of Geodesy and Geoinformation Science, Technische Universität Berlin, 10623 Berlin, Germany.

Color versions of one or more figures in this article are available at https://doi.org/10.1109/TGRS.2021.3062492.

Digital Object Identifier 10.1109/TGRS.2021.3062492

The precipitation signature was firstly seen in the measurements of the TechDemoSat-1 (TDS-1) satellite [7]. Based on a recent scattering model proposed in [8], the authors characterized the rain splash, the altered ocean roughness by the raindrops impinging on the surface, as a possible phenomenon reducing the received signal power at low wind speeds. This was also in agreement with the study discussing the roughness change as an increment of the sea surface slopes variance [9]. Later, a similar signature was also reported in CYGNSS measurements with the same explanation for the rain effects at low wind speeds [10]. At high winds, an underestimation of wind speed using CYGNSS measurements is reported which could be potentially due to the damping effect of rain on larger scale surface waves [11]. In a simulation study, it is shown that the atmospheric attenuation by raindrops is insignificant in space-borne GNSS-R L-band measurements [12]. This type of effect is expected to be even smaller in magnitude in ground-based GNSS-R observations (such as those in this study) due to the much shorter distance between the specular point and the receiver.

The previous studies have investigated the rain impact on GNSS-R measurements obtained by spaceborne receivers with nadir-looking left-handed circular polarization (LHCP) antennas. The impact on the scattered GNSS signals in right-handed circular polarization (RHCP) is still unknown. The depolarization effect by the flattening of the heavy precipitation is shown in polarimetric GNSS Radio Occultation measurements [13], but this type of effect in polarimetric GNSS-R data is not yet studied.

The objective of this study is not only to investigate the rain effects on polarimetric observations but also to further characterize the geophysical signatures and the interactions between rain and sea surface. Due to the lack of spaceborne polarimetric measurements, this study focuses on a ground-based experiment that can be potentially scaled up to spaceborne investigations in future. Section II discusses the physical theory and additionally, based on simulations, describes how the sea surface salinity (SSS) change due to rainfall could be potentially detectable using polarimetric observations. Section III explains the used data set for the empirical study. Section IV reports on the analysis, and finally Section V summarizes the results and gives the concluding remarks.

II. Physical Theory

A. Forward Models

The GNSS signals are originally transmitted in RHCP. Reaching the sea surface, part of the signals are bounced off in LHCP, while the rest keep their RHCP. The polarization ratio depends on the reflection geometry and sea surface permittivity. At elevation angles larger than the Brewster angle, the LHCP signal is dominant. If the reflection is recorded at an elevation angle lower than the Brewster angle, the majority of the signal remains at RHCP. Forward models, being valid only for ground-based observations, describe reflected RHCP and LHCP powers, $P^{\mathrm{r}}_{\mathrm{RHCP}}$ and $P^{\mathrm{r}}_{\mathrm{LHCP}}$, respectively, [14]

$$P^{r}_{\mathrm{RHCP}} = G^{\mathrm{ref}}_{\mathrm{RHCP}} |\Re_{\mathrm{RR}}| W^2 L^2 P_0 \tag{1}$$

$$P^{r}_{\mathrm{LHCP}} = G^{\mathrm{ref}}_{\mathrm{LHCP}} |\Re_{\mathrm{RL}}| W^2 L^2 P_0 \tag{2}$$

where G_{RHCP} and G_{LHCP} are the RHCP and LHCP antenna gains, P_0 is the incoming reference power at the receiver position, and W and L are the power loss due to insufficient delay-Doppler tracking of the reflected signal and surface roughness. Finally, $\Re$ is the polarization-dependent Fresnel reflection coefficient. Analogous to the polarization of incoming direct signals, there are two Fresnel coefficients. Co-polar coefficients, $\Re_{\mathrm{RR}}$ and $\Re_{\mathrm{LL}}$, and cross-polar coefficients, $\Re_{\mathrm{RL}}$ and $\Re_{\mathrm{LR}}$, can be obtained from the complex dielectric permittivity of sea surface water ϵ, and local elevation angle θ as follows [15]:

$$\Re_{\mathrm{RR}} = \Re_{\mathrm{LL}} = \frac{1}{2}(\Re_{\mathrm{VV}} + \Re_{\mathrm{HH}}) \tag{3}$$

$$\Re_{\mathrm{RL}} = \Re_{\mathrm{LR}} = \frac{1}{2}(\Re_{\mathrm{VV}} - \Re_{\mathrm{HH}}). \tag{4}$$

In the above equations, $\Re_{\mathrm{VV}}$ and $\Re_{\mathrm{HH}}$, polarization components parallel and perpendicular to the incidence plane, read

$$\Re_{\mathrm{VV}} = \frac{\epsilon \sin\theta - \sqrt{\epsilon - \cos^2\theta}}{\epsilon \sin\theta + \sqrt{\epsilon - \cos^2\theta}} \tag{5}$$

$$\Re_{\mathrm{HH}} = \frac{\sin\theta - \sqrt{\epsilon - \cos^2\theta}}{\sin\theta + \sqrt{\epsilon - \cos^2\theta}}. \tag{6}$$

Since P_0 is here unknown, we introduce the power ratios P_{RHCP} and P_{LHCP} as the observables

$$\begin{aligned} P_{\mathrm{RHCP}} &= P^{r}_{\mathrm{RHCP}}/P^{d} \\ &= \left(G_{\mathrm{RHCP}}/G^{d}\right)|\Re_{\mathrm{RR}}|^2 L^2 \end{aligned} \tag{7}$$

$$\begin{aligned} P_{\mathrm{LHCP}} &= P^{r}_{\mathrm{LHCP}}/P^{d} \\ &= \left(G_{\mathrm{LHCP}}/G^{d}\right)|\Re_{\mathrm{RL}}|^2 L^2 \end{aligned} \tag{8}$$

where P_0 is canceled out being divided by the power of direct signal $P^{\mathrm{d}} = G_d P_0$.

B. Salinity Change

As (5) and (6) imply, Fresnel coefficients are dependent on the relative permittivity of the seawater and the elevation angle of the signals. The permittivity of seawater is in turn controlled by the SSS and sea surface temperature (SST). The permittivity value can be obtained using models relying on the L-band measurements [16]–[18]. These models are used in ocean state retrievals using GNSS-R measurements [19]. Fig. 1 shows how SSS and SST changes can alter permittivity value based on simulations using the model proposed in [18]. As shown, at SSS values lower than almost 30 psu, which is the SSS range in the area studied in the following sections, the SSS plays a more significant role in controlling the permittivity value. The calculations using the Klein-Swift dielectric constant model confirm that the sensitivity of emissivity, and therefore reflectivity, to SST at L-band is insignificant also at higher SSS values and SSTs lower than 15 °C [20]. AQ:3

Conditions of SSS, considered in the following simulations, apply for the Western Baltic Sea where long-term GNSS-R measurements were conducted at the Onsala Observatory, discussed in the following sections. The historical observations of a station about 29-km away, between 2001 and 2009, show that there are large SSS variations around 25 psu remaining below 30 most of a year.

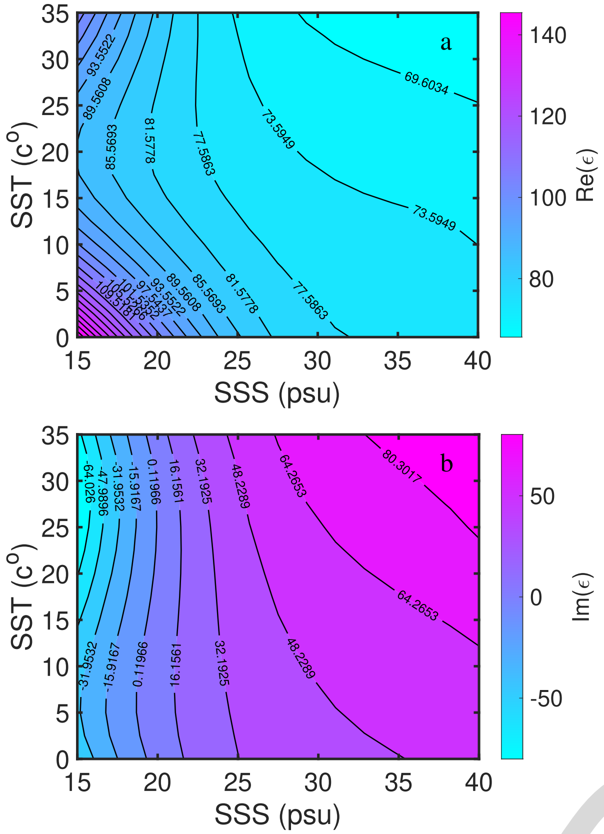

Fig. 1. (a) Real and (b) imaginary parts of dielectric permittivity of sea water versus SSS and SST.

Rain creates a fresher layer of water accumulating on the sea surface. This causes a rapid change in the SSS. The depth of the freshwater layer evolves, increasing or decreasing as a function of rain accumulation rate and sea state mixing the water. The mixing rate is in turn dependent on surface wind speed. So, more significant SSS changes are expected over a calm ocean, i.e., at low wind speeds. This has been also the condition providing the means to detect roughness change by rainfall, as discussed in [7].

Using a forward rain impact model (RIM), the SSS change is predictable as follows [21]:

$$S_{\mathrm{RIM}} = S_0 \left[\left(\prod_{i=1}^{n} \left[1 + \frac{R_{1i}}{\sqrt{k_z * t_i}} e^{-z^2/(4k_z t_i)} \right] \right) \right]^{-1} * \left[1 + \frac{R_2}{\sqrt{k_z * t}} e^{-z^2/(4k_z t)} \right]^{-1} \quad (9)$$

where S_{RIM} is the new salinity after precipitation, z is the depth in meters, n is the total number of rain events, S_0 is the initial salinity in psu, t is time in seconds, k_z is the vertical eddy diffusivity coefficient, R_{1i} and R_2 are the rain surface impulse function, the rain accumulation integrated over the characteristic mixing depth, for each event in meters. It is shown that the skin depth at the L-band frequency (1.4 GHz) and a fixed water temperature (20 °C) and salinity (34 psu) is 0.955 cm [22]. By definition, the skin depth is the medium thickness through which the electric field amplitude of the propagating electromagnetic wave falls to $1/e$, i.e., 37%, of its original value. Accordingly, the L-band penetration depth is not more than 1 cm, and we consider $z = 0.005$ m in this study.

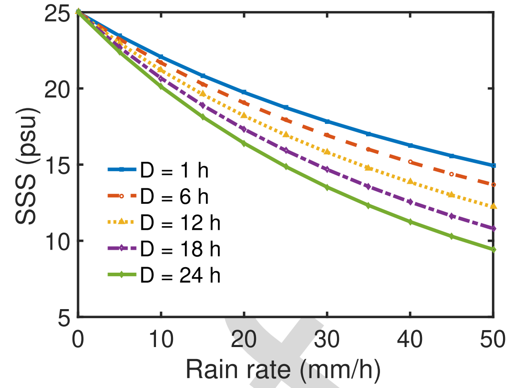

Fig. 2. SSS versus rain rate at different duration lengths (D) and $S_0 = 25$ psu.

Fig. 2 shows the SSS change due to rain events at different rates and duration (1, 6, 12, 18, and 24 h). For instance, the blue curve shows a 1-h rainfall at a constant rate of 10 mm/h drops the SSS from 25 psu to $\approx$ 24 psu. Following that, Fig. 3 shows the expected power levels and their ratio in these rain event scenarios. As demonstrated, altered SSS by rain could affect the observations at significant rain rates with a long enough duration. Besides, the power change for both RHCP and LHCP reflected GNSS signals and their ratio at different SSS values are illustrated in Fig. 4. As shown, significant drops of SSS are distinguishable in the power changes. This phenomenon increases the power of the LHCP signals, whereas, it decreases that scattered in RHCP. The discrepancy in the LHCP to RHCP power ratio will be therefore more significant leading to a more detectable SSS signature. This can be an advantage of polarimetric GNSS-R observations.

The RIM used here considers the surface salinity profile as a function of depth and time. Wind speed is not included and the model is assumed to describe the near-surface salinity profile at low wind speeds (0–3 m/s). The analysis in the following sections is conducted at a calm sea state. This is the condition in which the model is valid. Nevertheless, we should consider a level of uncertainty at different wind speeds. Besides, the wind might have a weaker effect in the coastal areas due to the land sheltering and the limited fetch [23], leading to a faster accumulation of the freshwater.

C. Roughness Change

When a raindrop impinges on the sea surface, a cavity with a crown is firstly created which will change to a vertical stalk at the center of rings of gravity-capillary waves. These waves propagate outwards, known as “ring waves” [24]. These small-scale waves alter the surface roughness which could affect the scatterometric measurements.

Numerous laboratory experiments are investigating the altered surface waves by rain. Based on them, theoretical models have been proposed to describe the generated waves and the impact on the surface, see, e.g., [25]–[28]. Although the ring waves intensify the centimeter-scale roughness, rain could also attenuate ocean surface gravity waves [27].

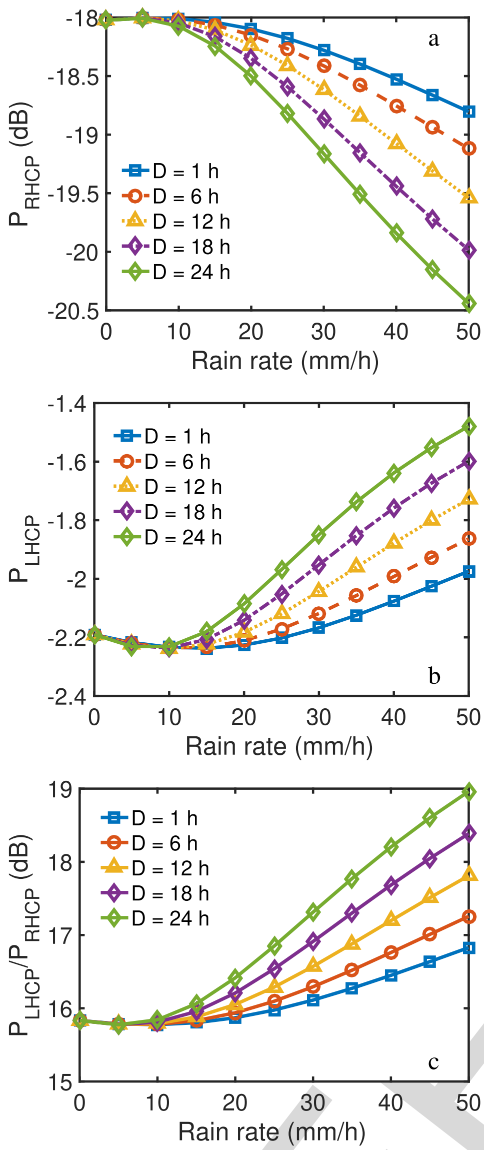

Fig. 3. Power of (a) reflected RCHP, (b) RHCP, and (c) signals and their ratio, and SST = 10 °C vs. rain rate at different rainfall duration lengths D, $\theta = 30°$, and $S_0 = 25$ psu.

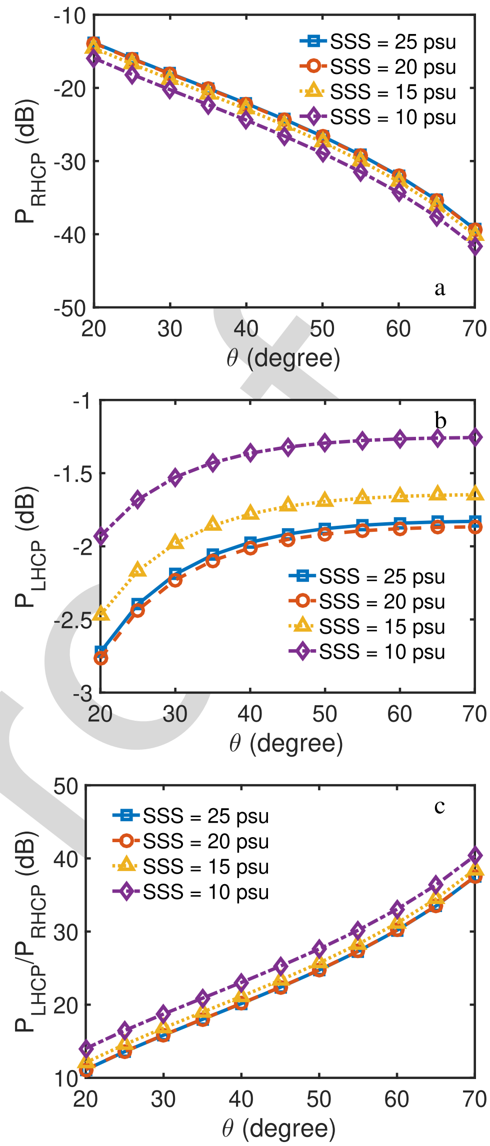

Fig. 4. Power of (a) reflected RCHP, (b) RHCP, and (c) signals and their ratio versus elevation angle θ at different SSS and SST = 10 °C.

The developed theories based on laboratory experiments do not yet sufficiently answer the questions on the mechanism of rain impact on ocean surface waves in real environments [29]. The simulations based on GNSS signal scattering models and the log Gaussian spectrum of rain-generated waves [28], do not show an exact match with the rain impacts observed in the empirical measurements [7]; however, the authors did not exclude the possibility of other effects existence such as swell and downdraft. In a recent study, field observations are used to describe rain impact on surface roughness [29]. Therein, more significant rain-enhanced gravity-capillary waves, with wavelengths smaller than $\lambda = 56$ mm are reported. These waves control the intensity of forward GNSS scattering in the regime of weak diffuse scattering, i.e., at low wind speed, which is the environmental condition for observing altered roughness effects in GNSS-R observations.

Further studies are required to characterize the rain-ocean interactions and consequently the effects on signal forward scattering patterns. We should therefore admit the effect of rain on the ocean surface is one of the least understood processes. We will discuss the result of this study on the surface change more in an empirical sense trying to enhance the knowledge on this process in a top-down approach.

In this study, the polarization-independent power loss due to the surface roughness is considered as [14]

$$L = \exp\left[(-1/2)\left(4\pi^2/\lambda^2\right)\sigma^2 \sin^2\theta\right] \qquad (10)$$

where σ is the standard deviation of sea surface height and λ is the wavelength of the GNSS signal. It should be noted that the power loss model described here applies to coherent scattering and does not account for possible polarization-dependent signatures of the roughness. This means the reflected signals can exhibit some degrees of ellipticity originated from the structure of the sea surface roughness. For instance, the horizontal parallel crests can act as an oriented structure affecting the horizontal component of the signals. Such roughness-induced polarimetric effects need to be further investigated in future studies.

Fig. 5. Eastward view of the GFZ GNSS-R station at (a) OSO, (b) zenith looking, RHCP, and side looking, RHCP and LHCP, antennas, and (c) sea targeted at the antenna boresight.

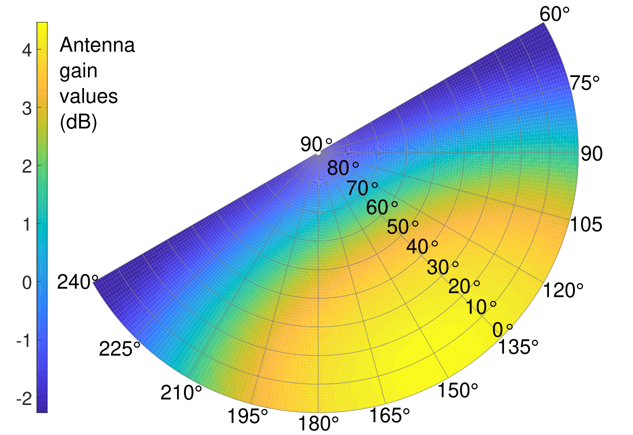

Fig. 6. Gain pattern of the reflectometry antennas as a function of satellite elevation and azimuth angles.

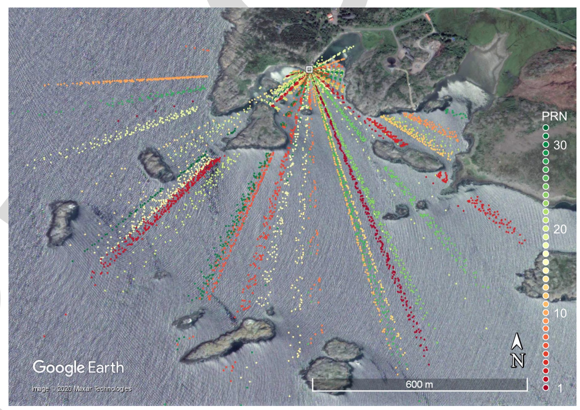

Fig. 7. Spatial extent of the specular points over the sea.

III. Experimental Data

A GFZ coastal GNSS-R station at Onsala Space Observatory (OSO) (57.393°N; 11.914°E) in Sweden is considered in this study for investigating the effect of precipitation on GNSS-R polarimetric observations. The data set covers a period of one year from January to December 2016. The station is equipped with a GNSS occultation, reflectometry, and scatterometry (GORS) receiver [30] with two reflectometry antennas in different polarization, i.e., RHCP and LHCP. The antennas are tilted $\approx 98°$ with respect to the zenith. The boresight of the reflectometry antennas is set at an azimuth angle of $\approx 150°$ to capture sea surface reflections with the highest gain values. The station environment and antennas are shown in Fig. 5.

The gain pattern of the antennas for incoming signals as a function of satellite elevation and azimuth angles is shown in Fig. 6. The experiment setup assigns high gains to the signals at grazing elevation angles, i.e., signals from satellites at 0° to about 40° elevation angles. The signals from the satellites with azimuth angles close to the antennas' boresight, i.e., 150°, are recorded at higher gains. The gain pattern is assumed to be equal for both the RHCP and LHCP sea-looking antennas.

The receiver uses designated channels to track the signals of the up-looking antenna (master channel) and side-looking antennas (slave channels), as previously described by [31]. In-phase and quadrature samples (I/Q) of the respective channels are recorded. Fig. 8 shows an example of the receiver output from the GPS satellite PRN 7 signals captured by the sea-looking antennas.

The antennas, here, have a small baseline ($\approx$20 cm) with respect to each other and are mounted with a height of about 3-m above the reflecting sea surface. For the given geometry the differential delay between direct and reflected signals cannot be resolved in the code delay domain. Multipath patterns of the direct and the reflected signals occur in the receiver output as previously explained, for example, by Larson *et al.* [32]. As shown in Fig. 8, a low-frequency pattern is evident in the interferometric pattern, which is attributed to the direct signal. A separation algorithm is applied to find the low-frequency pattern of the direct signal and the higher-frequency pattern of the reflected signal, as described by [33]. To be more specific, a first-order polynomial is fit to the low-frequency variations of I/Q correlation sum in each segment. Having the contribution

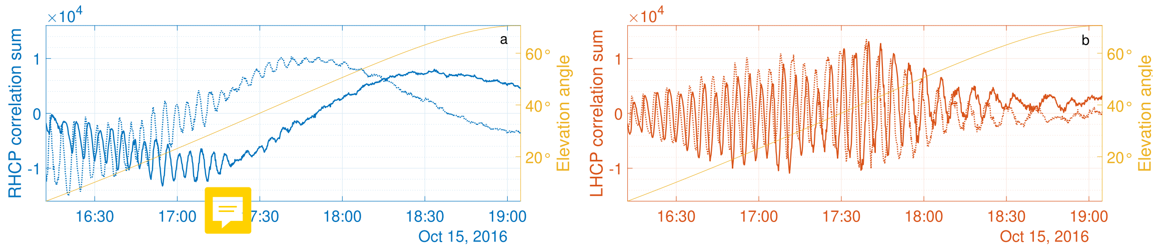

Fig. 8. Reflectometry observations of the GPS satellite PRN 7 on October 15, 2016, obtained from the Onsala station using two sea-looking antennas with right- and left-handed circular polarizations (RHCP and LHCP). The receiver output, i.e., the correlation sums, at in-phase and quadrature channels are shown as solid and dotted lines, respectively.

of the direct signal from this fitting, the I/Q contributions of the reflected signal is determined. For the here given geometry the separation algorithm yields estimates of the direct and reflected signal power every ten minutes.

The experiment uses wind, tide gauge, and precipitation measurements as the ancillary information for the analysis. The wind and sea-level measurements are obtained from the nearest meteorological and tide gauge stations, respectively. For the precipitation estimates, we use the GPM, half-hourly $0.1^\circ \times 0.1^\circ$ Version 06B Level 3 IMERG final run product.

The GNSS-R station can measure reflected signals at a sampling rate of 0.1 Hz from GPS satellites with elevation angles ranging from 0° to 50°. The spatial coverage of the specular points is shown in Fig. 7. During the one-year observation period, from January to December 2016, 175 178 measurements are recorded, from which 26 413 data are captured during rainfall, i.e., at rain rates higher than 0 mm/h. The maximum and average recorded rain rates are 23.04 and 0.09 mm/h, respectively.

IV. Analysis

Fig. 9 visualizes the power in both LHCP and RHCP versus the elevation angle along with simulated measurements using (1) and (2), derived from the entire data set. There is a general agreement between the observed and simulated measurements; however, the discrepancy of P_{RHCP} is larger compared to P_{LHCP}. Especially, there is a mismatch between the RHCP simulated and observed measurements at low elevation angles ($\lesssim 10^\circ$).

To investigate rain effects, the data are limited to wind speeds lower than 5 m/s as it is the necessary condition for detecting rain splash. Additionally, only the data at winds blowing from the land side, i.e., with azimuths between 0° and 150°, are considered. The location of the station and the considered azimuth range is shown in Fig. 10. In this condition, the wind-wave generation is limited by the short fetch. We use this sheltering effect of the coastline on the nearshore waves to further exclude wind-associated effects in the measurements. Then, this coastal experiment better provides the environmental conditions for tracking the rain splash effects compared to those using spaceborne measurements. Hoseini *et al.* [23] reported on the insignificant correlation between the offshore or land breeze and sea surface roughness at this GNSS-R station owing to the limited fetch. Furthermore, no meaningful correlation between precipitation and wind speed could be identified in our statistical analysis. The correlation coefficient between precipitation and wind speed is 0.1.

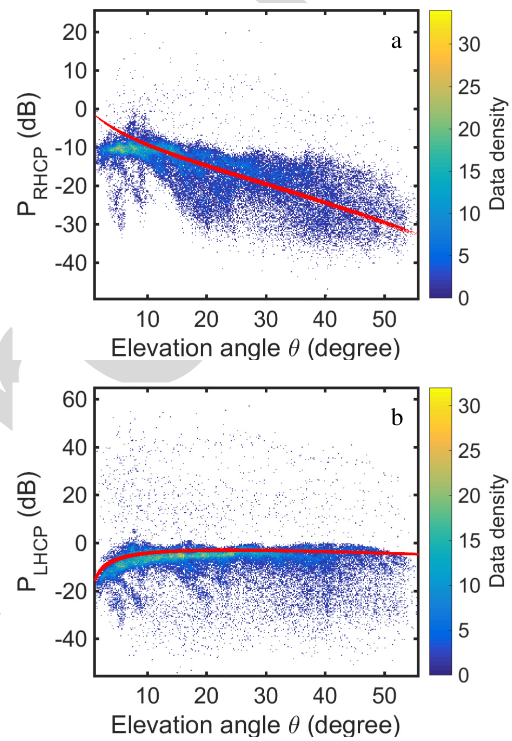

Fig. 9. Power of reflected (a) RCHP and (b) LHCP signals versus elevation angle θ along with simulated observations at $\sigma = 0.03$ m in red (entire data set). The SST values are obtained from a nearby meteorological station. The SSS for each observation is estimated as an average value based on historical records of between 2001 and 2009 at a station located about 29-km away.

Fig. 11 demonstrates the power of the reflected signal in both polarizations, in different cases, during rainfalls and rain-free measurements. A significant discrepancy between the two cases is shown which is larger at higher elevation angles. Besides, the simulations show the power behavior at different surface states. The similar patterns between the simulated and observed behavior show a possibility that the observed effects appear due to the rain splash altering the surface state, as discussed in [7]. In that spaceborne analysis, studying the intensity of the effect at different incidence angles was postponed to a future work due to the uncertainty of measurements. Here, the dependence of the rain effect on the reflection geometry is evident. We cannot exclude that the power drop in the empirical data might be intensified by other types of effects such as swell and downdraft which can be potentially the factors causing larger standard deviations during rainfall in Fig. 11. According to the figure, a higher level of sensitivity to rain in LHCP measurements is seen compared

Fig. 10. GNSS-R station location and the wind azimuth range condition (0°–150°) in the analysis.

to those RHCP observations. Besides, the probability density function (PDF) of the power measurements, derived as the kernel density estimation (KDE) is given in Fig. 12. It indicates that rain has distorted the PDF in both sets of measurements, dampening the peak and increasing the probability at lower values of power.

Fig. 13 shows the RHCP and LHCP reflection amplitudes at two different precipitation conditions during the setting period of the GPS satellite PRN 7. The shown exemplary cases do not necessarily meet the aforementioned conditions on the wind speed and its azimuth. Hence, wind speed and direction profiles are additionally given. The left column in the figure shows the I/Q components of the reflected signal during a rain-free period. As expected, a general trend of decreasing RHCP amplitude, and on the contrary, increasing LHCP amplitude over the satellite elevation angle is evident, which is due to the reflection geometry. Both cases are associated with offshore winds, so we expect to have a minimized wind-driven roughness effect. Fig. 13(a) on the left column reports on slightly higher wind speed. As a result, an insignificantly rougher sea surface with more power loss could be anticipated for the left column. The right column shows the case with the same GPS satellite and reflection geometry but during a rain-affected period.

Although the wind conditions might imply larger amplitude in rain-affected case, the RHCP and LHCP correlation sums in Fig. 13(d) and (f), exhibit smaller amplitudes leading to lower power ratios in Fig. 13(h). This power loss in the measurements of both polarizations compared to those in 13(g) can be explained with the rainfall. The striking fact is the systematic response to the rain rate in Fig. 13(h). There is an increase in the rain rate, from almost 0.5 to 3.6 mm/h, at elevation angles between 17° and 26°. The amplitudes shrink within this range along with a decrease in power ratios. The rain rate decrease also stimulates a relative increase in both of the power ratios when the satellite elevation angle passes 26°. However, the power ratios at elevation angles from 26° to 50° with a rain rate of 1.1 mm/h are slightly lower compared to the power ratios in Fig. 13(g). The amplitude change due to rain is more prominent in the LHCP observations compared to those in RHCP.

Considering the SSS change as the additional rain effect, we develop an inversion algorithm to estimate the standard deviation of surface heights and the SSS. $P_{\mathrm{RHCP}}(\sigma, S)$ and $P_{\mathrm{LHCP}}(\sigma, S)$ are considered as the observable parameters, see (7) and (8). The values of σ and S are sought which minimizes the cost function

$$\delta(\sigma, S) = \frac{1}{n}\sum_{i=1}^{n}\left|P^{o}_{\mathrm{RHCP},i} - P^{s}_{\mathrm{RHCP},i}(\sigma, S)\right| + \frac{1}{n}\sum_{i=1}^{n}\left|P^{o}_{\mathrm{LHCP},i} - P^{s}_{\mathrm{LHCP},i}(\sigma, S)\right| \quad (11)$$

where the superscripts o and s indicate the observed or simulated parameters, respectively. We assume that the variations of S and σ within 3 h are insignificant. So, these parameters are retrieved as the average value for every three-hour time span and n is the number of observations residing in each temporal bin. The conditions on the wind speed and its direction are applied here. Fig. 14 shows the obtained values for both parameters as a function of the rain rate.

According to Fig. 14, most of the data have a σ value of $\approx$ 3.5 cm. A steady increase in the average σ over the rain rate is observed with the correlation coefficient of 0.96. The derived SSS values show no significant trend at rain rates lower than 10 mm/h. Most of the data points, in a rain-free condition, reside at the SSS of $\approx$ 26 psu. A slight downward trend in the SSS at low rain rates, between 0 and 2.5 mm/h, is observed, decreasing the average SSS to $\approx$ 24 psu. Nevertheless, at higher rain rates up to 10 mm/h no significant change is observed in the average SSS value, which could statistically approve the SSS change due to rain. However, at rain rates larger than 10 mm/h a significant drop in the SSS values is observed.

The altered surface state and the effects on the power ratios shown here are much larger than the theoretical study on the surface effect of rain based on laboratory measurements, e.g., [28]. There is also a quantitative mismatch on the observed effects in TDS-1 and CYGNSS measurements with the theoretical studies [7], [10]. This inconsistency could be, at least partially, associated with the environmental differences between laboratory and real sea conditions. In a laboratory, the theoretical knowledge is derived based on observing wave parameters in a water tank influenced by artificially-generated rain and wind. Laxague and Zappa [29] discussed that the variation in such conditions is spatial, and not temporal. This is a considerable difference in a real sea, where rain may

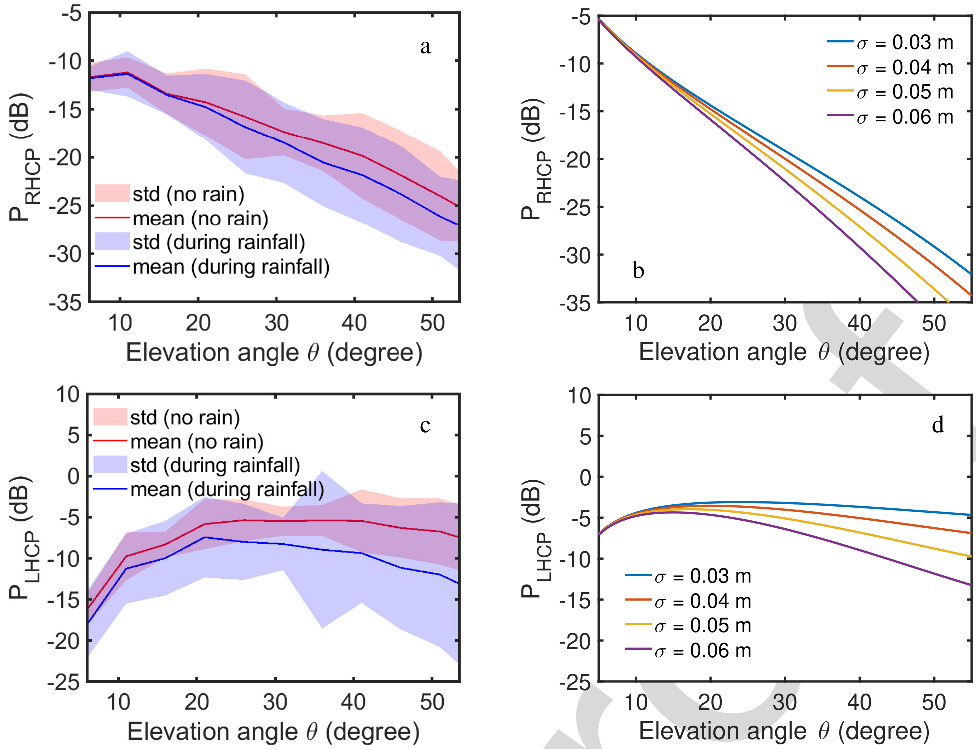

Fig. 11. (a) RHCP and (c) LHCP power ratios and in different cases, during rain events, at rates higher than 0.2 mm/h, and at no rain along with model-simulated (b) RHCP and (d) LHCP power ratios at different standard deviations of surface heights σ. Average and maximum rain rates of the data during rainfall are 1.5 and 23.0 mm/h, respectively.

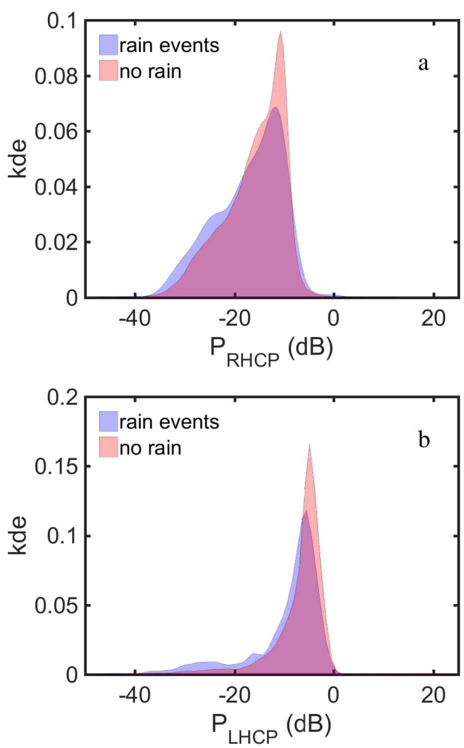

Fig. 12. PDF of (a) RCHP and (b) LHCP power in cases during rainfall and at no rain, derived as KDE.

affect the surface state rapidly, but environmental conditions do not vary spatially at a significant level for long periods. As a result, the laboratory-derived models are not satisfactory to characterize the problem of rain splash impacts on the sea surface waves and the change in the GNSS forward scattering patterns. *In situ* measurements of the impact of rain show a strong increase in the roughness in the scale of the gravity capillary waves with a wavelength between 5.4 and 56 mm [29]. These waves control the intensity of the reflection when the coherent component is considerable, i.e., when the wind speed is low and the Rayleigh parameter is large enough, see [7]. This is the condition applied to the analysis here.

The discussions in Section II theoretically prove the potential of simultaneous retrieval of SSS and surface state using polarimetric observations. The average values in Fig. 14 demonstrate the rain-associated systematic behaviors of these parameters. However, considerable uncertainties in σ and the SSS change are also seen which could be associated with different factors.

We cannot exclude non-rain environmental changes, such as swell and downdraft, which could still affect the retrievals and increase the uncertainty. We are not yet able to include all possible factors in the analysis since there is no readily available data set and method for parameterizing these complex processes. Additionally, we have visualized the impacts as a function of rain rate; however, the raindrop size and rainfall duration can impact the intensity of effects. It is known that larger raindrops can modify surface roughness more significantly, see, e.g., [34]. The raindrop size also controls the terminal velocity and, consequently, the downdraft intensity, see [10] and references therein. At low wind speeds such as those in the analysis here, small wave damping in the low-frequency band of wave spectrum might happen whose rate could increase as rain duration prolongs [35].

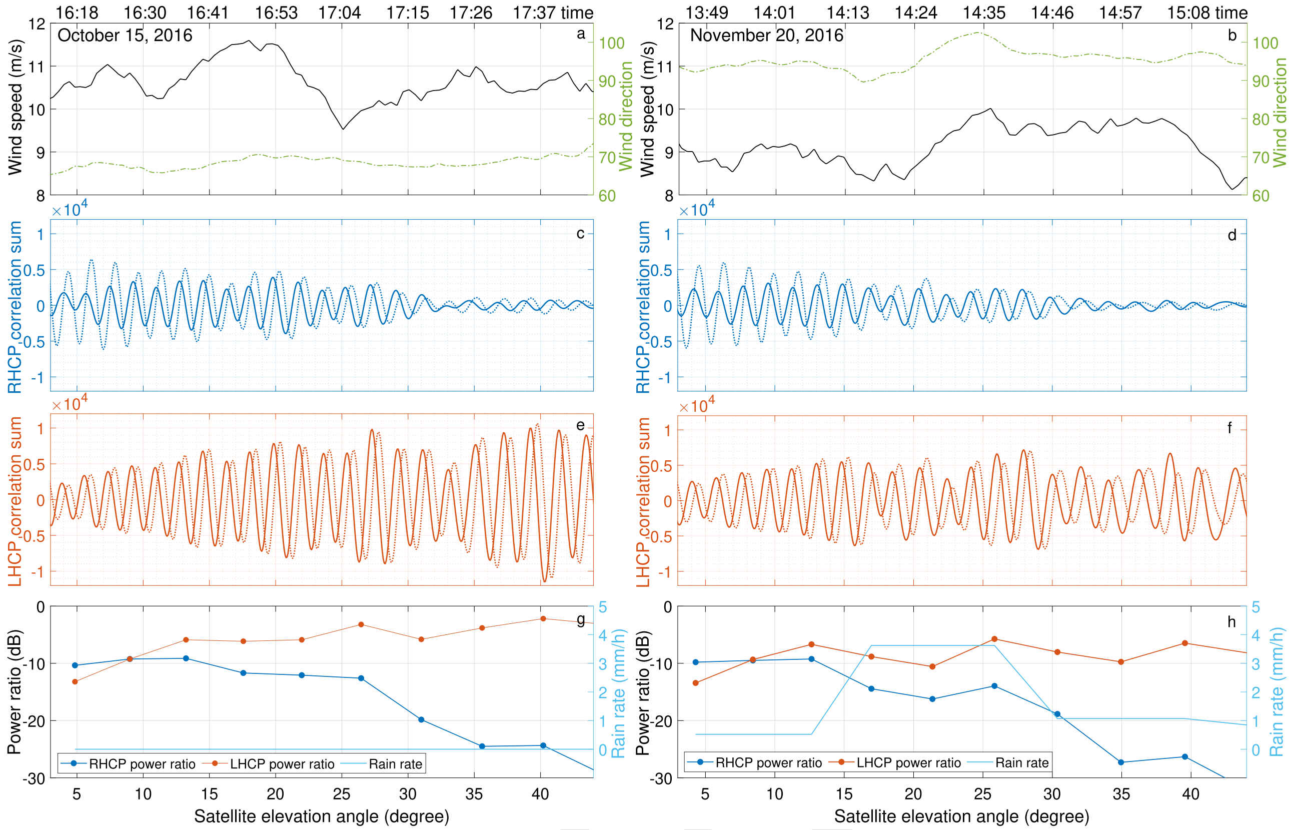

Fig. 13. Exemplary case of the rain impact on reflectometry observations from GPS satellite PRN 7. The graphs on the left side are related to the observations over a rain-free period. Right panels are associated with a time span that includes precipitation records based on the GPMs data. The reflectometry observations on both sides are selected to be over the same elevation angles of the satellite (a) and (b) wind speed and direction, (c) and (d) receiver output (correlation sums), quadrature in dotted and in-phase in solid line, from the RHCP antenna, (e) and (f) receiver output (correlation sums), quadrature in dotted and in-phase in solid line, from the LHCP antenna, and (g) and (h) ratios of the reflection power to direct signal power estimated from the RHCP and LHCP correlation sums against rain rate.

Besides, technical limitations should be considered. Here, the measurement noise might degrade the retrieval accuracy. A noise power analysis is carried out in [23] using the same data set. Noise power is calculated as the variance of quadrature components of the zenith-looking antenna over a temporal segment. Accordingly, the average noise power is in general between -1 and 0 dB, depending on the elevation angle. However, the standard deviation of the noise, varying between 2.5 and 3.5 dB, depending again on the elevation angle, is large enough to affect the retrieval.

Finally, we rely here on physical models by calculating the difference between observed and modeled powers in (11). Any inaccuracies in the models could also affect the retrieval efficiency. According to (10), the surface roughness is supposed to have a polarization-independent behavior. The empirical data demonstrate inconsistencies since the RHCP observations show a lower level of sensitivity to the roughness change compared to LHCP observations. The existence of this dependence is shown in Figs. 11 and 13. Fig. 15 shows the discrepancies between the modeled and observed LHCP to RHCP power ratio. According to the theoretical model, the ratio is supposed to be roughness-free, but here the roughness effect is evident, which is larger in magnitude at high elevation angles. The model has not been able to sufficiently describe the polarization-dependent results found, e.g., by [23] and [33] neither. Besides, the challenges on modeling and correcting the roughness effects to retrieve soil moisture is discussed by [36]. There is still a need and room for investigations on this topic.

This study has been focused on rain-caused modifications of reflecting surface properties. Intense rainfalls can additionally induce depolarization effects on the signals propagating through the atmosphere in grazing angle geometry due to the asymmetry between the horizontal and vertical dimensions of the big droplets. This effect has been studied in Radio Occultation [13], [37] and ground-based direct measurements [38]. The change in the ellipticity of the incoming circularly polarized signals could in turn affect the power estimations at intense rains and low elevation angles. In contrast, the studies here show that the observed signatures are more intense at high elevation angles and also noticeable at low rain rates. Although this implies that the ellipticity change of the incoming signal could not be the dominant type of effect causing the signatures observed here, we encourage characterizing this type of effect in future studies. There are still important questions on how thereby the GNSS-R observations are affected requiring decent investigations using optimized setups and analysis constraints for this purpose. Such an investigation is beyond scope of this article. The potential consequences in polarimetric GNSS-R measurements could be carried out in future studies with long

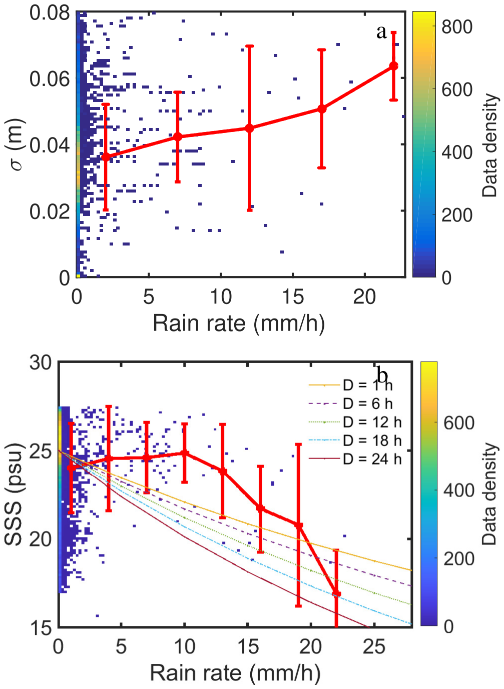

Fig. 14. Obtained values of (a) standard deviation of sea surface heights σ and (b) SSS along with simulated SSS at different rain duration D versus rain rate. The average values and standard deviations are shown in red.

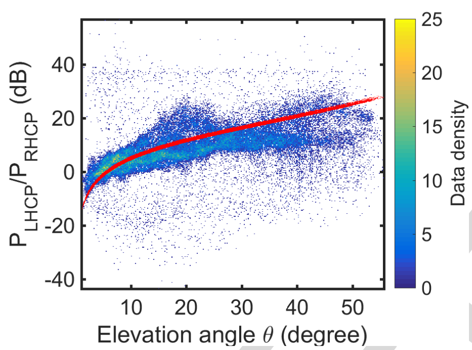

Fig. 15. LHCP to RHCP power ratio versus elevation angle along with simulations shown in red. The SST values are obtained from a nearby meteorological station. The SSS for each observation is estimated as an average value based on historical records of between 2001 and 2009 at a station located about 29-km away.

enough data sets especially with dense measurements at high rain rates.

V. Summary and Discussion

We investigated the response of polarimetric GNSS-R observations to precipitation for the first time. A discussion was made on the theoretical potential and the necessity of dual-polarization measurements for tracking the rain-caused SSS change in addition to sea surface modifications. The combination of the RHCP and LHCP observations amplifies the left signatures in the power ratios by the SSS change. Using a RIM, the change in the signal power due to SSS change is simulated which shows a considerable impact at high rain rates with long enough duration.

An analysis is carried out using measurements of a coastal GNSS-R station with two (RHCP and LHCP) side-looking antennas. The rain effects result in the discrepancy of the average power ratios in cases during rainfall and at no rain, which is proportional to the elevation angles. The geometry-dependence of the discrepancy magnitude implies a higher probability that the observed effects are mainly associated with the roughness change.

The left signature in both LHCP and RHCP power is large enough to be distinguishable in the measurements. The average LHCP power at an elevation angle of 45° drops by ≈ 5 dB; however, a significant increase in the standard deviation of the LHCP power is observed. In general, the LHCP observations enjoy a higher level of sensitivity to rain events, compared to RHCP measurements. This fact is further approved by investigating the amplitude of correlation sums in exemplary cases. The amplitude of the LHCP correlation sum shows more evident dampening by rainfall. This is a piece of evidence that the roughness loss is polarization-dependent, contrary to what the theoretical model implies. As a result, the models, especially those describing the power loss by the surface roughness, could be subjected to refinement in future studies.

An algorithm retrieving the SSS and surface state using the polarimetric measurements is proposed. The retrieved standard deviation of surface heights and the SSS also confirms that the general significant modification of the surface state, whereas, the SSS shows no meaningful behavior responding to rainfalls with rates below 10 mm/h. The retrieved SSS demonstrates a drop at higher rain rates. However, the data in this range are too sparse and studies with a substantially higher number of observations at extreme rain rates are encouraged and still required.

The reported roughness change by rain splash in this study is substantially larger than the modifications described by models derived based on laboratory measurements. We discussed that this can be due to the inefficiency of these models in describing the altered roughness in a real sea. The results show an agreement with recent *in situ* measurements in the real environment. This also explains the quantitative mismatch between the effects seen in the spaceborne measurements and model-based simulations in the previous studies.

None of the data sets used so far for the investigation of rain sensitivity are optimized for this purpose. Future investigations could be carried out on data sets from GNSS-R altimetry instruments due to the similarities of required environmental conditions, i.e., coherent reflections from calm surfaces. However, there is a dissimilarity in the desired reflection geometry. We are here interested in reflections at high elevation angles rather than those at grazing angles, considering the significant role of roughness change. The reflecting sea in the area of this study has smaller SSS values compared to global oceans remaining below 30 psu most of the time. In future studies on environments with higher SSS, SST change due to cold rainfalls can also be a significant research question over oceans with SSTs above 15 °C. The change in the ellipticity of the incoming circularly polarized signals propagating the rainy atmosphere deserves attention in future studies. With the derived knowledge in this study and previous investigations, we encourage future experiments fully dedicated to this topic.

Acknowledgment

The authors would like to thank Dr. Georg Beyerle at the German Research Centre for Geosciences (GFZ), Potsdam, Germany, for his contributions in this study and the Onsala Space Observatory (OSO) for hosting the GNSS Reflectometry (GNSS-R) station. They would also like to thank the Swedish Meteorological and Hydrological Institute (SMHI) and the team associated with NASA's global precipitation measurement (GPM) Mission for the ancillary data used in this investigation.

References

[1] S. M. Papalexiou and A. Montanari, "Global and regional increase of precipitation extremes under global warming," *Water Resour. Res.*, vol. 55, no. 6, pp. 4901–4914, May 2019.

[2] G. J. Huffman *et al.*, "The TRMM multisatellite precipitation analysis (TMPA): Quasi-global, multiyear, combined-sensor precipitation estimates at fine scales," *J. Hydrometeorol.*, vol. 8, no. 1, pp. 38–55, Feb. 2007.

[3] A. Y. Hou *et al.*, "The global precipitation measurement mission," *Bull. Amer. Meteorol. Soc.*, vol. 95, pp. 701–722, May 2014.

[4] Q. Sun, C. Miao, Q. Duan, H. Ashouri, S. Sorooshian, and K. Hsu, "A review of global precipitation data sets: Data sources, estimation, and intercomparisons," *Rev. Geophys.*, vol. 56, no. 1, pp. 79–107, Mar. 2018.

[5] V. U. Zavorotny, S. Gleason, E. Cardellach, and A. Camps, "Tutorial on remote sensing using GNSS bistatic radar of opportunity," *IEEE Geosci. Remote Sens. Mag.*, vol. 2, no. 4, pp. 8–45, Dec. 2014.

[6] C. S. Ruf *et al.*, "A new paradigm in Earth environmental monitoring with the CYGNSS small satellite constellation," *Sci. Rep.*, vol. 8, no. 1, Dec. 2018, Art. no. 8782.

[7] M. Asgarimehr, V. Zavorotny, J. Wickert, and S. Reich, "Can GNSS reflectometry detect precipitation over oceans?" *Geophys. Res. Lett.*, vol. 45, no. 22, 2018, Art. no. 12585.

[8] A. G. Voronovich and V. U. Zavorotny, "The transition from weak to strong diffuse radar bistatic scattering from rough ocean surface," *IEEE Trans. Antennas Propag.*, vol. 65, no. 11, pp. 6029–6034, Nov. 2017.

[9] A. Camps *et al.*, "Determination of the sea surface emissivity at L-band and application to SMOS salinity retrieval algorithms: Review of the contributions of the UPC-ICM," *Radio Sci.*, vol. 43, no. 3, pp. 1–16, 2008.

[10] R. Balasubramaniam and C. Ruf, "Characterization of rain impact on L-band GNSS-R ocean surface measurements," *Remote Sens. Environ.*, vol. 239, Mar. 2020, Art. no. 111607.

[11] E. Cardellach, Y. Nan, W. Li, R. Padullés, S. Ribó, and A. Rius, "Variational retrievals of high winds using uncalibrated CyGNSS observables," *Remote Sens.*, vol. 12, no. 23, p. 3930, Nov. 2020.

[12] M. Asgarimehr, J. Wickert, and S. Reich, "Evaluating impact of rain attenuation on space-borne GNSS reflectometry wind speeds," *Remote Sens.*, vol. 11, no. 9, p. 1048, May 2019.

[13] E. Cardellach *et al.*, "Sensitivity of PAZ LEO polarimetric GNSS radio-occultation experiment to precipitation events," *IEEE Trans. Geosci. Remote Sens.*, vol. 53, no. 1, pp. 190–206, Jan. 2015.

[14] F. G. Nievinski and K. M. Larson, "Forward modeling of GPS multipath for near-surface reflectometry and positioning applications," *GPS Solutions*, vol. 18, no. 2, pp. 309–322, Apr. 2014.

[15] V. U. Zavorotny and A. G. Voronovich, "Scattering of GPS signals from the ocean with wind remote sensing application," *IEEE Trans. Geosci. Remote Sens.*, vol. 38, no. 2, pp. 951–964, Mar. 2000.

[16] L. Klein and C. Swift, "An improved model for the dielectric constant of sea water at microwave frequencies," *IEEE J. Ocean. Eng.*, vol. 2, no. 1, pp. 104–111, Jan. 1977.

[17] T. Meissner and F. J. Wentz, "The complex dielectric constant of pure and sea water from microwave satellite observations," *IEEE Trans. Geosci. Remote Sens.*, vol. 42, no. 9, pp. 1836–1849, Sep. 2004.

[18] Y. Zhou, R. H. Lang, E. P. Dinnat, and D. M. Le Vine, "L-band model function of the dielectric constant of seawater," *IEEE Trans. Geosci. Remote Sens.*, vol. 55, no. 12, pp. 6964–6974, Dec. 2017.

[19] C. Ruf *et al.*, *CYGNSS Handbook*, vol. 154. Ann Arbor, MI, USA: Michigan, 2016.

[20] D. M. Le Vine and E. P. Dinnat, "The multifrequency future for remote sensing of sea surface salinity from space," *Remote Sens.*, vol. 12, no. 9, p. 1381, Apr. 2020.

[21] A. Santos-Garcia *et al.*, "Investigation of rain effects on aquarius sea surface salinity measurements," *J. Geophys. Res., Oceans*, vol. 119, no. 11, pp. 7605–7624, Nov. 2014.

[22] M. D. Anguelova and P. W. Gaiser, "Skin depth at microwave frequencies of sea foam layers with vertical profile of void fraction," *J. Geophys. Res.*, vol. 116, no. C11, 2011.

[23] M. Hoseini *et al.*, "On the response of polarimetric GNSS-reflectometry to sea surface roughness," *IEEE Trans. Geosci. Remote Sens.*, early access, Nov. 2, 2020, doi: 10.1109/TGRS.2020.3031396.

[24] A. M. Worthington, *A Study Splashes*. London, U.K.: Longmans, Green, and Company, 1908.

[25] L. F. Bliven, P. W. Sobieski, and C. Craeye, "Rain generated ring-waves: Measurements and modelling for remote sensing," *Int. J. Remote Sens.*, vol. 18, no. 1, pp. 221–228, Jan. 1997.

[26] L. F. Bliven, H. Branger, P. Sobieski, and J.-P. Giovanangeli, "An analysis of scatterometer returns from a water surface agitated by artificial rain: Evidence that ring-waves are the main feature," *Int. J. Remote Sens.*, vol. 14, no. 12, pp. 2315–2329, Aug. 1993.

[27] Y.-K. Poon, S. Tang, and J. Wu, "Interactions between rain and wind waves," *J. Phys. Oceanogr.*, vol. 22, no. 9, pp. 976–987, Sep. 1992.

[28] C. Craeye, P. W. Sobieski, and L. F. Bliven, "Scattering by artificial wind and rain roughened water surfaces at oblique incidences," *Int. J. Remote Sens.*, vol. 18, no. 10, pp. 2241–2246, Jul. 1997.

[29] N. J. M. Laxague and C. J. Zappa, "The impact of rain on ocean surface waves and currents," *Geophys. Res. Lett.*, vol. 47, no. 7, Apr. 2020, Art. no. e2020GL087287.

[30] A. Helm *et al.*, "The GNSS occultation, reflectometry, and scatterometry space receiver GORS: Current status and future plans within GITEWS," in *Proc. 1st Colloq., Sci. Fundam. Aspects Galileo Programme*, Toulouse, France, 2007, pp. 1–4.

[31] A. M. Semmling *et al.*, "A zeppelin experiment to study airborne altimetry using specular global navigation satellite system reflections," *Radio Sci.*, vol. 48, no. 4, pp. 427–440, Jul. 2013.

[32] K. M. Larson, E. E. Small, E. Gutmann, A. Bilich, P. Axelrad, and J. Braun, "Using GPS multipath to measure soil moisture fluctuations: Initial results," *GPS Solutions*, vol. 12, no. 3, pp. 173–177, Jul. 2008.

[33] A. M. Semmling *et al.*, "Sea-ice concentration derived from GNSS reflection measurements in fram strait," *IEEE Trans. Geosci. Remote Sens.*, vol. 57, no. 12, pp. 10350–10361, Dec. 2019.

[34] D. Houk and T. Green, "A note on surface waves due to rain," *J. Geophys. Res.*, vol. 81, no. 24, pp. 4482–4484, 1976.

[35] R. Rajesh Kumar, B. Prasad Kumar, and D. Bala Subrahamanyam, "Parameterization of rain induced surface roughness and its validation study using a third generation wave model," *Ocean Sci. J.*, vol. 44, no. 3, pp. 125–143, Sep. 2009.

[36] A. Camps, H. Park, J. Castellví, J. Corbera, and E. Ascaso, "Single-pass soil moisture retrievals using GNSS-R: Lessons learned," *Remote Sens.*, vol. 12, no. 12, p. 2064, Jun. 2020.

[37] E. Cardellach *et al.*, "Sensing heavy precipitation with GNSS polarimetric radio occultations," *Geophys. Res. Lett.*, vol. 46, no. 2, pp. 1024–1031, Jan. 2019.

[38] H. An, W. Yan, S. Bian, and S. Ma, "Rain monitoring with polarimetric GNSS signals: Ground-based experimental research," *Remote Sens.*, vol. 11, no. 19, p. 2293, Oct. 2019.

Milad Asgarimehr received the M.Sc. degree in geodesy from the K. N. Toosi University of Technology, Tehran, Iran, in 2015, and the Ph.D. degree (Hons.) from the German Research Foundation (DFG), in 2020.

Being awarded a Ph.D. Fellowship by X. Geo, the geoscientific competence network in Berlin, Germany, and Potsdam, Germany, he joined the German Research Centre for Geosciences (GFZ), Potsdam, and the Technische Universität Berlin, Berlin, in 2017. His Ph.D. dissertation was dedicated to the GNSS Reflectometry and remote sensing of the ocean and atmosphere. He is a Post-Doctoral Researcher with GFZ. His main research interests include bistatic radar, the development of novel remote sensing techniques, and studying Earth systems using the derived data especially with the help of artificial intelligence.

Dr. Asgarimehr was awarded the Bernd Rendel Prize in geosciences by DFG.

Mostafa Hoseini graduated in geodesy from the University of Tehran, Tehran, Iran.

He has worked for several institutions as a GNSS Engineer in the field of positioning and navigation. Before starting his Ph.D. studies in 2018 at the Norwegian University of Science and Technology (NTNU), Trondheim, Norway, he worked on the analysis of GNSS atmospheric products at the German Research Centre for Geosciences (GFZ), Potsdam, Germany. His research interest includes GNSS-based sensors and techniques for remote sensing applications. His research interest also includes the monitoring of the ocean and Arctic using GNSS-Reflectometry onboard CubeSats.

Maximilian Semmling graduated in physics from Leipzig University, Leipzig, Germany, in 2007. He received the Ph.D. degree from Technische Universität Berlin, Berlin, Germany, in 2012.

For his doctoral and post-doctoral studies, he was with the German Research Centre for Geosciences (GFZ), Potsdam, Germany, the Institute for Space Studies of Catalonia (IEEC), Barcelona, Spain, and the University of the Littoral Opal Coast (ULCO), Dunkirk, France. In 2020, he joined the Observation Department, German Aerospace Center (DLR), Institute for Solar-Terrestrial Physics, Neustrelitz, Germany. He is experienced in GNSS for Earth observation with a research focus on ocean altimetry and sea ice remote sensing. His work concentrates on the influence of atmosphere and space weather. Corresponding methods cover a wide range from ground-based measurements over maritime, and airborne to satellite platforms.

Markus Ramatschi graduated in geophysics in 1992. He received a Ph.D. degree in geophysics from the Technical University of Clausthal, Clausthal-Zellerfeld, Germany, in 1998.

Since 2000, he has been the Senior Scientist of the German Research Centre for Geosciences (GFZ), Potsdam, Germany. His work focuses mainly on the operation of GNSS sensor stations and related hardware developments.

Adriano Camps (Fellow, IEEE) was born in Barcelona, Spain, in 1969.

In 1993, he joined the Electromagnetics and Photonics Engineering Group, Department of Signal Theory and Communications, Universitat Politècnica de Catalunya (UPC), Barcelona, as an Assistant Professor, an Associate Professor in 1997, and a Full Professor since 2007. In 1999, he was on sabbatical leave at the Microwave Remote Sensing Laboratory, the University of Massachusetts at Amherst, Amherst, MA, USA. He has published more than 223 articles in peer-reviewed journals, eight book chapters, and the book, Emery and Camps, *Introduction to Satellite Remote Sensing. Atmosphere, Ocean, Land and Cryosphere Applications* (Elsevier, 2017, 860 pages), and more than 471 conference presentations. He holds 12 patents. He has advised 27 Ph.D. Thesis students (+eight on-going) and more than 140 final project and M.Eng. theses. According to Google Scholar/Scopus his H-index is 52/40. His research interests include microwave remote sensing, with special emphasis in microwave radiometry by aperture synthesis techniques (MIRAS instrument onboard ESA's SMOS mission), remote sensing using signals of opportunity (GNSS-R), and nanosatellites as a tool to test innovative remote sensors.

Dr. Camps has received several awards, among which the European Young Investigator Award in 2004, the ICREA Academia Research Award in 2009 and 2015, and the Duran Farell Award for Technology Transfer in 2000 and 2010.

Hossein Nahavandchi received the Ph.D. degree from the Royal Institute of Technology (KTH), Stockholm, Sweden, in 1998.

He is a Professor of geodesy and geophysics with the Norwegian University of Science and Technology (NTNU), Trondheim, Norway. His research interests include global geodetic observations systems (GGOSs), including satellite gravimetry, satellite altimetry, satellite radar interferometry, and GNSS to understand the dynamic Earth system by quantifying Earth's change in space and time.

Rüdiger Haas received the M.Sc. and Ph.D. degrees in geodesy from Bonn University, Bonn, Germany.

He is a Full Professor of space geodesy with the Department of Space, Earth and Environment, Chalmers University of Technology, Gothenburg, Sweden. He is also the Head of the Research Group for Space Geodesy, Chalmers, and responsible for the geoscience activities at the Onsala Space Observatory. His research interests include space geodetic techniques, such as global navigation satellite systems (GNSSs), including GNSS-reflectometry, and very long basline interferometry (VLBI).

Jens Wickert received the Diploma degree in physics from Technical University Dresden, Dresden, Germany, in 1989, and the Ph.D. degree in geophysics/meteorology from Karl-Franzens University Graz, Graz, Austria, in 2002.

He was the Principal Investigator of the pioneering GPS radio occultation experiment aboard the German CHAllenging Minisatellite Payload (CHAMP) Satellite and coordinates numerous research projects on GNSS remote sensing. He holds a joint professorship of German Research Centre for Geosciences (GFZ), Potsdam, Germany, with the Technical University of Berlin, Berlin, Germany, on global navigation satellite systems (GNSSs) remote sensing, navigation, and positioning. He is also the Deputy GFZ Section Head of Space Geodetic Techniques and the GFZ Research Topic Director of The Atmosphere in Global Change. He has authored or coauthored more than 250 Web of Science indexed publications on GNSS Earth observation.